HHS Public Access

Author manuscript

Sci Transl Med. Author manuscript; available in PMC 2024 May 20.

Published in final edited form as:

Sci Transl Med. 2024 April 24; 16(744): eadk6213. doi:10.1126/scitranslmed.adk6213.

Single-cell multiomics guided mechanistic understanding of Fontan-associated liver disease

Po Hu[1,2,3,8], **Jack Rychik**[4], **Juanjuan Zhao**[1,2,3], **Huajun Bai**[1,2,3], **Aidan Bauer**[1,2,3,8], **Wenbao Yu**[5,7], **Elizabeth B. Rand**[4], **Kathryn M. Dodds**[4,6], **David J. Goldberg**[4], **Kai Tan**[5,7], **Benjamin J. Wilkins**[3], **Liming Pei**[1,2,3,8,9,10,*]

[1]Center for Mitochondrial and Epigenomic Medicine, Children's Hospital of Philadelphia; Philadelphia, PA 19104, USA

[2]Cardiovascular Institute, Children's Hospital of Philadelphia; Philadelphia, PA 19104, USA

[3]Department of Pathology and Laboratory Medicine, Children's Hospital of Philadelphia; Philadelphia, PA 19104, USA

[4]Department of Pediatrics, Children's Hospital of Philadelphia; Philadelphia, PA 19104, USA

[5]Center for Childhood Cancer Research, Children's Hospital of Philadelphia; Philadelphia, PA 19104, USA

[6]School of Nursing, Perelman School of Medicine, University of Pennsylvania; Philadelphia, PA 19104, USA

[7]Department of Pediatrics, Perelman School of Medicine, University of Pennsylvania; Philadelphia, PA 19104, USA

[8]Department of Pathology and Laboratory Medicine, Perelman School of Medicine, University of Pennsylvania; Philadelphia, PA 19104, USA

[9]Institute for Diabetes, Obesity, and Metabolism, Perelman School of Medicine, University of Pennsylvania; Philadelphia, PA 19104, USA

[10]Cardiovascular Institute, Perelman School of Medicine, University of Pennsylvania; Philadelphia, PA 19104, USA

Abstract

The Fontan operation is the current standard of care for single-ventricle congenital heart disease. Individuals with a Fontan circulation (FC) exhibit central venous hypertension and face life-threatening complications of hepatic fibrosis, known as Fontan-associated liver disease (FALD). The fundamental biology and mechanisms of FALD are little understood. Here we generated the

*Corresponding author. lpei@pennmedicine.upenn.edu.

Author contributions: L.P. conceived and directed the project. P.H., J.Z. and H.B. performed experiments and analyzed the data. J.R. provided the liver samples from patients with Fontan operation and helped with data interpretation. A.B. provided technical assistance. W.Y. and K.T. provided assistance in data analysis. D.J.G., E.B.R. and K.M.D. helped procure the liver samples and interpret the cardiovascular and liver data. B.J.W. is a pathologist who examined the histological and immunohistochemistry studies. P.H. and L.P. wrote, and all authors reviewed or edited the manuscript.

Competing interests: J.R. is a consultant for NUVO Cares. D.J.G. is a consultant for Inozyme Pharma. The authors declare that they have no other competing interests.

first transcriptomic and epigenomic atlas of human FALD at single-cell resolution using multiomic snRNA-ATAC-seq. We discovered profound cell type-specific transcriptomic and epigenomic changes in FC livers. Central hepatocytes (cHep) exhibited the most significant changes, featuring profound metabolic reprogramming. These cHep changes preceded substantial activation of hepatic stellate cells and liver fibrosis, suggesting cHep as a potential first “responder” in the pathogenesis of FALD. We also identified a network of ligand-receptor pairs that transmit signals from cHep to hepatic stellate cells, which may promote their activation and liver fibrosis. We further experimentally demonstrated that Activins A and B promote fibrotic activation *in vitro* and identified mechanisms of Activin A’s transcriptional activation in FALD. Together, our single-cell transcriptomic and epigenomic atlas revealed mechanistic insights into the pathogenesis of FALD and may aid identification of potential therapeutic targets.

One Sentence Summary:

A single-cell multiomics atlas of FALD reveals mechanisms of disease pathogenesis.

INTRODUCTION

The Fontan operation is the current standard of care for single-ventricle congenital heart disease (SVCHD), a category of congenital cardiac anomalies in which there is only one functional ventricle. First introduced over fifty years ago, the Fontan operation has undergone improvements and refinements which now allow for survival of the majority of children with SVCHD. It is estimated that there are approximately 80,000 survivors of this procedure worldwide (1). Importantly, the surgical strategy is not curative and results in a unique physiological state of chronic venous hypertension and relatively low cardiac output, which is the foundation for multiple end-organ complications (2). Despite the diverse etiologies of the original SVCHD, a universal complication and one of the most concerning is hepatic fibrosis, now recognized as FALD (3). FALD often leads to liver cirrhosis, which increases the risk of hepatocellular carcinomaand can require liver transplantation at young ages, thus increasing morbidity and limiting mid-to long-term overall survival for those born with SVCHD (4–6).

FALD is a “new” disease that has only become recognized and characterized recently due to the survival of a growing number of individuals with FC. It is now recognized that FALD is morphologically, and presumably mechanistically, distinct from other well-studied forms of liver fibrotic disease, such as alcoholic liver disease (ALD) or metabolic dysfunction-associated steatohepatitis (MASH, previously referred to as non-alcoholic steatohepatitis or NASH) (7). It has been suggested that liver fibrosis may result from dysregulation of biological processes due to the hemodynamic derangements inherent in the FC such as elevated central venous pressure. As there are currently no animal models for FALD, fundamental mechanisms underlying FALD remain poorly understood. One strategy to improve our understanding is to explore FALD from the cellular perspective. It is plausible to suspect that cell type-specific remodeling occurs in FC livers, including substantial modifications in transcriptional and epigenetic states that drive functional changes underlying the observed pathophysiology. An improved understanding of the

primary and likely causal events, preferably at single-cell resolution, could offer crucial insights into FALD etiology that could then lead to development of targeted therapies.

Technological advances in droplet microfluidics, sequencing and bioinformatics in recent years have enabled massively parallel single-cell or single-nucleus transcriptome and epigenome analysis of tens of thousands of cells or nuclei (8). Such single-cell or single-nucleus RNA sequencing (scRNA-seq or snRNA-seq) or Assay for Transposase-Accessible Chromatin using sequencing (scATAC-seq or snATAC-seq) technologies empower genome-wide transcription and epigenetics analysis, respectively, at the single-cell resolution, and have provided insights into many areas of biology such as cellular identity, heterogeneity, and gene regulatory mechanisms. For example, detailed gene expression and epigenomic states of cells from multiple organs of a whole organism, including human and mouse, can now be studied at single-cell resolution (9–12). Furthermore, we can now simultaneously interrogate both the transcriptome and epigenome from the same cell using multiomic snRNA-ATAC-seq. Understanding complex diseases such as FALD at the single-cell resolution will reveal cellular heterogeneity and cell type-specific transcriptional changes, crucial insights unavailable from traditional bulk sequencing approaches. Single-cell multiomics such as snRNA-ATAC-seq will further uncover potentially causal gene regulatory mechanisms underlying such cell type-specific transcriptional changes.

In this study, we generated the first transcriptomic and epigenomic atlas of human FALD at single-cell resolution with multiomic snRNA-ATAC-seq. The results revealed profound cell type-specific transcriptional and epigenetic changes in FC livers as well as transcription factors potentially mediating these changes. We also set out to uncover the network of ligand-receptor pairs that potentially promote hepatic stellate cell (HSC) activation and liver fibrosis and validated them *in vitro*. Together, this single-cell transcriptomic and epigenomic atlas revealed new mechanistic insights into the underlying pathogenesis of FALD as well as potential therapeutic targets.

RESULTS

The single-cell transcriptomic atlas of human FALD

Our goal was to discover early and likely causal changes underlying the pathogenesis of FALD. We therefore carefully screened patients with FC at the Children's Hospital of Philadelphia (CHOP) based on the results of their comprehensive clinical evaluation, with detailed characterization of the cardiovascular system and various end organs. We identified four patients who all underwent a Fontan operation at 2-3 years of age, and who had liver biopsies obtained when they were teenagers (13-18 years old). At the time of liver biopsy, they exhibited normal ventricular function by echocardiography and mild hepatic pathology based on liver ultrasound and histological examination of the biopsy samples (table S1). All patients with FC underwent concomitant cardiac catheterization at time of liver biopsy, with demonstration of elevated inferior vena cava and hepatic wedge pressures (table S1). Two age-matched resected liver samples (13-14 years old) with confirmed normal liver histology were used as controls. After quality filtering (minimum of 800 genes and 800 ATAC peaks detected per nucleus), nuclei containing high-quality data of both transcriptome and epigenome (10,726 for control and 16,047 for Fontan) were retained for further analysis.

A technical challenge in analyzing single-cell genomics data, particularly in human clinical samples, is the batch effect resulting from often unavoidable technical variations such as sample availability time, anatomical location of biopsy, inter-individual variation, inter-experiment variations in library preparation and sequencing parameters. Although many methods have been developed to minimize the batch effects of single-modal datasets such as snRNA-seq data (13, 14), reliable data integration methods that effectively minimize the batch effect of multimodal datasets such as snRNA-ATAC-seq data are still being developed. To overcome this challenge, we first used Harmony (15) to integrate the transcriptome portion of our multiomic snRNA-ATAC-seq data to minimize batch effects (fig. S1A). This allowed us to unambiguously identify 7 clusters/cell types in both control and FC livers based on their transcriptome profiles: cHep, portal hepatocyte (pHep), HSC, endothelial cell (EC), macrophage, lymphocyte, and cholangiocyte (Fig. 1, A and B). The numbers of detected transcripts (unique molecular identifiers), genes, and ATAC peaks per nucleus were comparable among all cell types (fig. S1B). The 7 liver cell types exhibited distinct gene expression signatures defining their identities (Fig. 1, C and D, and fig. S1C). cHep and pHep were the most abundant, representing ~80% of the total nuclei. Changes in cell type composition between control and FC livers were not statistically significant (fig. S1, D and E).

Cell type-specific liver transcriptional remodeling in human FALD

We next compared differential gene expression for individual liver cell types between control and FC livers. Although the main clinical feature of FALD is fibrosis, believed to result from HSC activation, cHep exhibited the biggest transcriptional changes, with 1,124 genes increased or decreased in FC livers (Fig. 2A). In contrast, only 145 pHep genes were differentially expressed. This suggests that elevated central venous pressure caused by FC exerts differential impacts on the two hepatocyte populations, with cHep being anatomically closer to the central vein and thus affected to a greater degree. Gene ontology (GO) analysis revealed profound metabolic reprogramming in FC cHep, with significantly elevated expression of genes important in small-molecule metabolism such as Acyl-CoA oxidase 2 (*ACOX2*, $P<1.4x10^{-244}$), xenobiotic response such as Alcohol Dehydrogenase 1C (*ADH1C*, $P<1.3x10^{-59}$), and cellular oxidoreductive activity such as Catalase (*CAT*, $P<2.3x10^{-308}$) (Fig. 2, B and C).

Differential gene expression was also observed in HSCs and other liver cell types, but to a much lesser extent. HSC is generally believed to be the major liver cell type that synthesizes and deposits extracellular matrix directly contributing to fibrosis. HSCs showed modestly increased expression of only a small number of extracellular matrix genes and those involved in cellular response to transforming growth factor beta (TGFβ) such as *COL6A1* and *COL4A4* (Fig. 2, B and C). We further experimentally validated these gene expression results by qPCR (fig. S1E), and by immunohistochemistry to determine Catalase protein abundance (Fig. 2D).

The single-cell epigenomic landscape of human FALD

By studying the same high-quality nuclei as shown in Fig. 1, A and B, we analyzed the epigenome (ATAC) portion of the multiomic snRNA-ATAC-seq data, using Harmony to

integrate and minimize batch effects. Epigenomic data alone was sufficient to resolve the liver cell types, except for setting a clear boundary between cHep and pHep. Based on both the cluster-specific peaks (fig. S2) and joint transcriptome-based identity of individual nucleus 7 clusters were found to unambiguously represent the same 7 liver cell types: cHep, pHep, HSC, EC, macrophage, lymphocyte and cholangiocyte (Fig. 3, A and B). All 7 liver cell types exhibited distinct epigenetic signatures, such as increased accessibility of the promoter or enhancer regions of cell type-specific genes (Fig. 3C and fig. S2, comparing to Fig. 1C).

We also discovered differentially accessible genomic regions for individual liver cell types between control and FC livers. Similar to the gene expression changes, cHep exhibited the greatest epigenomic changes, with 118 differentially accessible genomic regions in FC livers (Fig. 4A). In particular, the 47 genomic regions with increased accessibility were found to be statistically associated with metabolic genes such as those important in small-molecule metabolism (Fig. 4B), consistent with the metabolic reprograming in FC cHep at the transcriptional level.

Our multiomic snRNA-ATAC-seq data allowed us to analyze the transcriptome and linked epigenome from the same cell, revealing the underlying regulatory mechanisms of cell type-specific transcriptional changes in FALD. We focused on understanding the profound metabolic reprogramming in cHep. We investigated the epigenetic signatures of all metabolic genes that exhibited increased expression in FALD cHep. Overall, 704 cHep genes showed increased expression and 47 cHep genes showed increased chromatin accessibility (Fig. 4A), with 17 genes showing both increased expression and increased chromatin accessibility (fig. S3A). These 17 genes, including *ABCC6, ACAA1, ADH4, CYP2C8*, and *HAAO*, are mostly involved in metabolic processes (fig. S3B). We further examined all 17 genes and found that there were no newly opened chromatin regions in FALD cHeps; rather, these open regions were relatively more accessible (increased height/areas). A coverage plot of a representative gene (*ABCC6*) is shown to illustrate this point (fig. S3C). We expanded joint transcriptome-epigenome analyses to all upregulated metabolic genes in FALD cHeps, such as *ADH4* (Fig. 4C). cHep-aggregated ATAC signals identified multiple accessible regions (ATAC peaks) at the human *ADH4* locus, including the promoter and potential enhancers. By analyzing the co-variation (correlation) between *ADH4* promoter activity and chromatin accessibility of individual ATAC peaks at each single cell and across all cHep cells while controlling for technical biases in chromatin accessibility measurements, we identified potential enhancer regions that are crucial for increased *ADH4* expression. For example, this analysis revealed several enhancer regions of *ADH4* important for its increased expression in FALD cHep, with an enhancer immediately downstream of the last exon (*) showing the strongest correlation (Fig. 4C). By analyzing the DNA sequences of these *ADH4* promoter and enhancer peaks and applying the same method for all metabolic genes with increased expression in FALD cHep (Fig. 2B), we found that they were statistically enriched for DNA-binding motifs of many transcription factors (table S2). By filtering out those either not expressed or barely expressed in FALD cHeps, the top transcription factor motifs included those found in PPARγ, SP3, NRF1 (nuclear respiratory factor 1, not to be confused with nuclear factor erythroid-derived 2-related factor 1 or NFE2L1), NR2C2, NFYC, PPARα, and ZNF148 (Fig. 4D). All

these transcription factors also showed increased expression in FC cHeps (fig. S4). The importance in hepatocyte metabolism or even liver fibrosis has been documented for some of these transcription factors (PPARγ, PPARα, and NR2C2) (16–20), whereas it remains to be definitively determined for others (SP3, NRF1, NFYC, and ZNF148). In summary, our unbiased analyses based on snRNA-ATAC-seq results suggest that these transcription factors most likely mediate cHep metabolic reprogramming in FALD.

cHep signaling to HSCs promotes HSC activation and liver fibrosis in human FALD

Our snRNA-ATAC-seq results reveal that cHeps exhibit the biggest transcriptomic and epigenomic changes. This likely reflects the fact that cHeps are anatomically closer to the central vein and therefore most affected by the FC-induced elevation of central venous pressure. In contrast, pHeps show little changes. Additionally, only very minor activation of HSC and liver fibrosis, based on the above transcriptomic and epigenomic results, is occurring at this stage of FALD. These results point to cHep as possibly the first “responder” to FC which then “transmits” signals to HSC, resulting in the known FALD pathology including HSC activation, collagen production and deposition, and liver fibrosis. Therefore, we next used the snRNA-ATAC-seq data to uncover possible intercellular signaling axes (ligand-receptor pairs) between different liver cell types with a focus on signals from cHep to HSC (Fig. 5A). We found more than 100 ligand-receptor pairs where ligands and receptors were highly expressed in cHep and HSC, respectively (table S3), and some of these ligand-receptor pairs showed increased expression in FALD. For example, the activin family ligands *INHBA, INHBB* and *INHBC* (encoding Activin A, B and C proteins, respectively) all showed significantly increased expression in cHep, whereas their receptors *ACVR1B, ACVR2A* and *ACVR2B* showed significantly increased expression in HSC in FALD (Fig. 5B).

We further tested whether this ligand-receptor signaling may activate HSC. We treated the human fibroblast cell line MRC-5, which is highly responsive to TGFβ, with different ligand proteins. We found that Activin A and B, but not Activin C, dose-dependently induced expression of fibrotic genes such as *ACTA2* and *COL4A1* to an extent comparable to TGFβ (Fig. 5C). In addition, Activin A and B, but not Activin C, also increased ACTA2 protein abundance to an extent comparable to TGFβ (Fig. 5D).

We next investigated the regulatory mechanisms of increased expression of these ligands, focusing on *INHBA*. Our snATAC-seq data identified NRF1 and ZNF148 binding sites in an ATAC peak in the promoter region of the *INHBA* gene. Re-analysis of published NRF1 ChIP-seq (21) and H3K27Ac ChIP-seq data (22) further supported the binding of NRF1 to this *INHBA* promoter (Fig. 5E; unfortunately no ZNF148 ChIP-seq data is published yet). We next tested whether NRF1 and ZNF148 could bind to the *INHBA* promoter and induce its expression. We cotransfected the human *INHBA* promoter with different transcription factors (NRF1, ZNF148, and PPARα) in human HEK293T cells and luciferase reporter assays confirmed that both NRF1 and ZNF148, but not PPARα, strongly induced *INHBA* promoter activity (Fig. 5F). Together, these results highlight the value of our snRNA-ATAC-seq data in discovering crucial mechanisms of pathogenesis of FALD and potential therapeutic targets.

Distinct mechanisms of FALD compared to other liver fibrosis diseases

FALD is morphologically different, and we have discovered here that it is also mechanistically distinct from other liver fibrotic diseases such as MASH. MASH is a more severe form of liver disease that often includes clinical features of substantial metabolic dysregulation, inflammation, and fibrosis. Single-cell genomics studies of human/mouse MASH that included unbiased analysis of all liver cell types were recently reported (23–27). To further understand the common and unique pathogenesis and mechanisms of FALD, we reanalyzed the raw data from a recent study that produced one of the most comprehensive human MASH snRNA-seq data to date (27) and conducted a detailed comparison with our FALD snRNA-ATAC-seq results.

Our analysis revealed that, unlike FALD studied here which primarily exhibits changes specific in cHeps, MASH is characterized by extensive changes across multiple cell types (Fig. 6). There was a considerable overlap of upregulated genes in cHeps between MASH and FALD. However, this overlap was minimal in other cell types such as pHeps, lymphocytes, ECs, and cholangiocytes. The common differentially expressed genes in cHeps were associated with various metabolic pathways including increased monocarboxylic metabolism, small molecular metabolism, biological oxidations, lipid biosynthesis and modification (Fig. 6A). In addition, cHeps in FALD exhibited a substantial increase in organic hydroxy compound metabolism and hormone metabolism. These changes occurred without any increase in inflammatory response and platelet metabolism as observed in cHeps in MASH. In contrast to cHeps, there was minimal overlap of differentially expressed genes in pHeps between MASH and FALD (Fig. 6A). In MASH, pHeps demonstrated an increase in acute-phase response and xenobiotic stimulus response, whereas pHeps in FALD exhibited similar metabolism pathways as observed in FALD cHeps.

Consistent with the fibrosis phenotype, both FALD and MASH showed a considerable upregulation of genes related to extracellular matrix remodeling and organization. These changes were mainly attributed to HSCs (Fig. 6B). One of the most notable differences between FALD and MASH was the substantial inflammation observed in MASH but not in the stage of FALD studied. Many inflammatory and immune pathways were prominent in MASH and involved several cell types including cHeps, lymphocytes, and ECs (Fig. 6C). Inflammation was largely absent at the stage of FALD studied based on our snRNA-ATAC-seq data and consistent with clinical observation. Overall, the minimal overlap of differentially expressed genes in ECs, HSCs, lymphocytes, and cholangiocytes also suggests that distinct pathways are activated in MASH and FALD, respectively. These results further strengthen our conclusion that FALD is a unique human liver disease featuring a distinct underlying molecular etiology.

DISCUSSION

Here we generated a single-cell transcriptomic and epigenomic atlas of human FALD. Our results revealed profound cell type-specific changes in the livers of individuals with FC. Our two most important findings are that first, among all liver cell types, cHeps exhibited the most significant transcriptional and epigenetic changes, featuring profound metabolic reprogramming. This suggests that cHep may be a potential first “responder” in

the pathogenesis of FALD. Second, we identified cHep→HSC signals that potentially drive HSC activation and liver fibrosis in FALD. Based on these findings, we propose a model for the pathogenesis of FALD (fig. S5).

FALD remains little understood and current clinical diagnosis and research often focus on the fibrosis aspect. Our results showed that at the stage of FALD studied, the major molecular changes were occurring in cHep, not in HSC. In fact, cHep alone represented nearly half of total transcriptomic (42%) and epigenomic (46%) changes in all 7 liver cell types combined. These cHep changes seemed to precede substantial HSC activation and liver fibrosis. These results strongly suggest that cHep is primary and central to the etiology of FALD, and cHep reprogramming might be a causal feature to FALD pathophysiology. If confirmed in future studies with clinical samples from additional SVCHD forms and Fontan procedures, we should consider cHep metabolic changes as a key feature of FALD. This may lead to the development of quantitative biomarker means for more accurate diagnosis and potential therapies for FALD treatment.

Recent serum metabolomics studies have indicated significant changes in circulating concentrations of acylcarnitines, amino acids, lipids, and bile acids in patients with FC (28–30). These results are generally consistent with our single-cell data. Future studies using liver metabolomics will further link liver metabolite changes to metabolic transcriptional/epigenetic changes (our snRNA-ATAC-seq data) and the reported plasma metabolomics results (28–30). This will determine whether and how muchliver metabolic changes contribute to circulating metabolomics alterations in patients with FC.

An outstanding question is why cHeps may mediate the first causal changes of FALD. The sharp contrast of transcriptomic and epigenomic changes between cHeps and pHeps offers important clues to this question. Although molecularly and functionally close, an important difference is that cHeps are anatomically adjacent to the central vein. Elevation of central venous pressure is a key component of FC and has been thought to be important for FALD development. Therefore, an enticing hypothesis is that the first important step of FALD pathogenesis is that chronic elevation of central venous pressure results in or facilitates profound transcriptional and epigenetic changes in cHep (Fig. S5). Further evidence supporting this hypothesis is that the EC population, which includes ECs also anatomically close to the central vein, exhibited the 2nd biggest transcriptomic changes among all liver cell types. Similarly to cHeps, ECs could potentially directly sense the central venous pressure changes and transmit signals to HSC and others to contribute to liver fibrosis.

Joint epigenome analysis from the same cell provided mechanistic insights into the metabolic reprogramming of cHep. These analyses suggested that transcription factors PPARγ, SP3, NRF1, NR2C2, NFYC, PPARα, and ZNF148 may mediate these metabolic gene expression changes. PPARγ and PPARα are well established as important regulators of multiple metabolic pathways, including in the liver (31, 32). Hepatocyte-specific loss of PPARγ results in substantial changes in liver metabolism, especially lipid metabolism (16–18). PPARα and pan-PPAR agonists are being tested in clinical trials for treating MASH (33, 34). NRF1 is a crucial regulator of mitochondrial biogenesis and function,

thereby impacting cellular metabolism (35, 36), but its specific role in liver metabolism and fibrosis has not been fully determined. Nuclear receptor NR2C2 regulates lipid metabolism, and whole-body *Nr2c2* KO mice are protected from obesity-induced inflammation and hepatic steatosis (19, 20). The functional importance of SP3, NFYC, and ZNF148 in liver metabolism and fibrosis remains to be established. Future cHep- or hepatocyte-specific gain- and loss-of-function studies will further define the importance of these factors in regulating hepatocyte metabolism and liver fibrosis.

Overall, we identified fewer differentially accessible chromatin regions than differentially expressed genes in all liver cell types in FALD. Published bulk or single-cell ATAC-seq data suggest that significant chromatin accessibility changes often occur when there are cell identity changes, such as during embryonic development, cell differentiation, or reprogramming. In contrast, much smaller chromatin accessibility changes occur when it involves cell states or functional changes. For example, a recent scATAC-seq study in a mouse liver regeneration model (featuring moderate cell identity changes) revealed a total of 551 differentially accessible chromatin regions across three time points (37). Another bulk ATAC-seq study of liver steatosis and MASH (featuring few cell identity changes, similar to FALD) showed only 49 and 190 differentially accessible chromatin regions in steatosis and MASH, respectively, compared to normal livers (38). Our results in FALD are largely consistent with this notion and literature.

Furthermore, by analyzing cell-cell interactions using our snRNA-ATAC-seq data, we identified the network of ligand-receptor pairs that transmit signals from various liver cell types, particularly cHeps to HSCs, which might promote their activation and liver fibrosis. We further experimentally validated that Activins A and B promote HSC activation *in vitro*. It was recently shown that both hepatic and circulating Activin B are increased in patients with MASH and alcoholic cirrhosis, and neutralizing Activin B with antibodies largely prevented liver fibrosis in the CCl_4-induced liver injury mouse model (39). Another recent study indicated that Activin A can activate HSCs indirectly through inducing TNFα and TGFβ in Kupffer cells (liver macrophages) (40). We took a further step and identified that NRF1 and ZNF148 are induced in FALD cHeps, which in turn activate the transcription of *INHBA* (which encodes Activin A). There are currently no animal models for FALD that recapitulate its unique pathophysiology and underlying mechanisms. When such models become available in the future, it will be important to test whether inhibiting Activin A, B, or other crucial pathways reported here represent potential treatment strategies for FALD.

By comparing the single-cell genomics data of FALD and MASH, we have uncovered both common and unique biological aspects of these conditions. Overall, MASH involves broad changes in many cell types, whereas cHeps are the primary cell type exhibiting the most substantial changes in FALD. The cHeps of FALD and MASH share some common metabolic reprogramming, but also display unique alterations. One of the most notable differences is that the inflammatory response is highly upregulated across many cell types in MASH, but is absent in FALD. A caveat to this comparison is that the FALD samples used in our study are most likely at the early stage of the disease, whereas MASH is often considered an advanced stage of liver disease. Nonetheless, the similarities and differences

between FALD and MASH further reinforce that FALD is a unique human liver disease with a distinct underlying molecular etiology.

In summary, our single-cell transcriptomic and epigenomic atlas reveals new mechanistic insights into the pathogenesis as well as potential therapeutic targets of FALD. We further experimentally validated some of the most important new findings. Important future research directions include further determining how cHep metabolic reprogramming is induced by elevated central veinous pressure, and whether targeting cHep metabolic dysregulation and key cHep to HSC signaling pathways (such as Activins A or B) mitigates liver fibrosis and allow for prevention or treatment of FALD.

MATERIALS AND METHODS

Study design

FALD is a disease that has only been recognized in the last few decades with the invention and success of the Fontan operation in saving babies with SVCHD. Despite its high prevalence and severe consequence, its underlying biology and mechanism of pathogenesis are little understood. In this study, we aimed to fill this knowledge gap with the hope of advancing scientific understanding to eventually help patients with FALD. As there are currently no animal models of FALD, studying human samples is the only and probably best option. Our approach leveraged single-cell multiomics technology to reveal the transcriptomic and epigenomics changes from the same cell. This allowed us to understand for the first time the molecular events happening in FALD, gain mechanistic insights, experimentally validate them, and based on these results propose a model of FALD pathogenesis.

For liver biopsy samples reflective of the FC population, we leveraged a state-of-the-art specialized multidisciplinary clinic at the Children's Hospital of Philadelphia (CHOP), the FORWARD (Fontan rehabilitation, wellness and resilience development) program. Here, patients with FC routinely undergo a comprehensive clinical evaluation with detailed characterization of the cardiovascular system and various end organs. At a period of greater than 10 years from Fontan operation, the FORWARD program clinic offers detailed surveillance assessments of FALD, which includes hemodynamic characterization through cardiac catheterization and simultaneous percutaneous liver biopsy evaluations (41, 42). The protocols for human liver sample and data collection, including informed consent received prior to participation, are approved by the CHOP Institutional Review Board (IRB 20-017749). We carefully screened recent patients with FC based on results of their comprehensive clinical evaluation and identified 4 patients who all underwent a Fontan operation at 2-3 years of age and had liver biopsies when they were teenagers (13-18 years old). At the time of liver biopsy, they exhibit only mild hepatic pathology based on liver ultrasound and histological examination of the biopsy samples. All 4 patients underwent concomitant cardiac catheterization at the time of liver biopsy, with demonstration of elevated inferior vena cava and hepatic wedge pressures (table S1).

Another important factor in our study design is to obtain age- and sex-matched control liver samples. Human liver biopsy samples are difficult to obtain, especially for teenagers.

This is particularly true for healthy control liver samples due to obvious ethical reasons. We obtained two resected liver samples from age-matched children. We further confirmed that they possessed normal liver histology. We carefully evaluated additional resected liver samples available that were from ~2-year-old children. They appeared to have many proliferating cells and less mature hepatocytes. We therefore decided to exclude such age-mismatched control samples in our study. We reasoned against increasing the FALD sample size at this point as the bottleneck was the limited number of teenage control liver samples. All control and FALD samples were procured and processed as carefully and fast as possible (described below) to minimize impact of sample processing and inter-sample variation.

In addition, experiments that validated the most important mechanistic insights obtained from the snRNA-ATAC-seq study were performed in biological replicates and repeated at least twice to ensure rigor and reproducibility.

Human tissue procurement and processing

Liver biopsy of ~1mm x 1mm x 1cm was obtained, immediately put on ice, and transferred to the pathology lab. Part of the liver biopsy was fixed and sectioned for pathology diagnosis by pathologists and for immunohistochemistry, and the rest was immediately frozen in liquid N2 for snRNA-ATAC-seq. The clinical metadata of the 4 patients with FC in this study are presented in table S1. Control liver samples are healthy liver adjacent to resected malignancy from donors of similar age. Frozen human liver samples were homogenized in 0.1X lysis buffer (10mM Tris-HCl, 10mM NaCl, 3mM $MgCl_2$, 1% BSA, 1mM DTT, 0.1% Tween-20, 0.1% NP-40, 0.01% Digitonin, 1U/μl RNase inhibitor) using a Dounce Homogenizer (Active Motif, 40401), followed by 5 min of incubation on ice. Nuclei quality was examined under microscope after this step. Next, nuclei were centrifuged at 500 rcf for 5 min at 4°C. Supernatant was carefully disregarded, and nuclei were resuspended in 500ul pre-chilled wash buffer containing 10mM Tris-HCl, 10mM NaCl, 3mM $MgCl_2$, 1% BSA, 1mM DTT, 0.1% Tween-20, and 1U/μl RNase inhibitor. The washing step was repeated twice. After washing, all nuclei passed through 40μm Flowmi cell strainer (Bel-Art, H13680-0040). After nuclei concentrations were counted, nuclei were resuspended in nuclei buffer (10x Genomics) with the final concentrations for all six sample (2 control + 4 FC livers) approximately 2,000 – 3,000 nuclei/μl.

snRNA-ATAC-seq and initial data processing

Isolated nuclei were immediately processed following the Chromium Next GEM Single Cell Multiome ATAC + Gene expression protocol. 6,000 – 13,000 nuclei from each sample were used to perform transposition and partitioned into gel beads and barcoded using 10x Genomics Chromium controller. The barcoded and transposed DNA was pre-amplified and ATAC library was constructed using appropriate sample index following the Chromium Next GEM Single Cell Multiome ATAC User Guide. Meanwhile, cDNA was amplified and purified using pre-amplified DNA (the same DNA constructing the ATAC library) and Gene Expression library was constructed using appropriate sample index following the Chromium Next GEM Single Cell Multiome Gene expression User Guide. Both ATAC and Gene Expression Library qualities were confirmed using Bioanalyzer DNA Kits (Agilent, 5067-4626) and 2100 Bioanalyzer (Agilent, G2939BA). Furthermore, libraries

were quantified using KAPA Library Quantification Kit and sequenced using Illumina NovaSeq 6000 (100 cycles) with 28:10:10:90 paired-end cycles format for Gene Expression library and 50:8:24:49 paired-end cycles format for ATAC library.

snRNA-ATAC-seq data were first demultiplexed using the *mkfastq* function of cellranger-arc (v2.0.0) and then further processed using count function of cellranger-arc (v2.0.0). All reads were aligned to the reference GRCh38 genome cellranger-arc (v2.0.0). snRNA-seq data of each sample were processed using Seurat (v4). Nuclei with fewer than 800 unique molecular identifiers (likely low quality) and greater than 20,000 unique molecular identifiers (likely multiplets) were removed from downstream analysis. In addition, we also filtered out cells with more than 10% of unique molecular identifiers mapped to the mitochondrial genome. The filtered snRNA-seq data of each sample were saved individually as a Seurat object. snATAC-seq data of each sample was processed by scATAC-pro (v1.4.2) (43), using the FASTQ and fragments files generated by cellranger-arc (v2.0.0). The peaks and cells were called by default methods and parameters. Nuclei with fewer than 800 or greater than 10,000 ATAC read counts were also removed from downstream analysis. The nucleus by peak count matrix was used for downstream analysis. As a result, 3263 and 7463 nuclei with high quality RNA and ATAC data were retained in the 2 control liver samples, respectively, whereas 3392, 4340, 5711, and 2604 nuclei with high quality RNA and ATAC data were retained in the 4 FC liver samples, respectively.

snRNA-seq data integration

snRNA-seq data of two control liver samples were merged into one Seurat object (Control) using *merge* function in Seurat. Meanwhile, the same method was applied to merge snRNA-seq data of four Fontan liver samples into another Seurat object (Fontan). Next, we normalized each Seurat object using the *NormalizeData* function and performed Principal Component Analysis (PCA) using the *RunPCA* in Seurat with 50 principal components (PCs). To tackle the batch correction, we further harmonized Control and Fontan Seurat objects separately using the *RunHarmony* function, followed by clustering using the *FindNeighbors* and *FindClusters* functions in Seurat. The resulting clusters were visualized using Uniform Manifold Approximation and Projection (UMAP) via the *RunUMAP* function in Seurat with default settings. The 10,726 Control nuclei were classified into 7 clusters with the resolution parameter set to 0.25 and the 16,047 Fontan nuclei were classified into 7 clusters with the resolution parameter set to 0.1. The cluster violin plots, feature plots, and heat maps were generated as we previously described (44).

Identification of differentially expressed genes between Control and Fontan liver

Differential gene expression of individual cell type between Control and Fontan livers was identified via the *FindMarkers* function in Seurat, using LR (likelihood ratio) test. Genes with a fold-change of more than 1.5 and a P-value less than $1x10^{-5}$ were considered differentially expressed. We used Metascape (metascape.org) to perform GO enrichment analysis for differentially expressed genes using the default setting (performed in Nov 2022).

snATAC-seq data integration

snATAC-seq data from Control and Fontan samples, respectively, were integrated by scATAC-pro '*integrate*' module with parameter 'Integrate_by=harmony', which generated a Seurat object using the union of peaks called from all Control or Fontan samples as features. UMAP was constructed on the first 30 Harmony components. Differentially accessible peaks were identified using the *FindMarkers* function in Seurat by the default setting. Gene activity matrices were extracted from differentially accessible peaks by using the *GeneActivity* function in the Signac R package (45). We used Metascape (metascape.org) to perform GO enrichment analysis for differential gene activity using the default setting.

snRNA-ATAC-seq data integration

For each sample, we used the cell barcodes as the shared cell barcodes between snRNA-seq and snATAC-seq data. We added a chromatin assay into the snRNA-seq Seurat object using the *CreateChromatinAssay* function in Signac. We also used the *CreateFragmentObject* function in Signac to add the fragments file into the merged Seurat object. We then merged all Seurat objects from Control or Fontan samples for predicting gene-peak links and visualization. The gene-peak links were predicted using the *LinkPeaks* function in Signac and the links were visualized using the *CoveragePlot* function in Signac.

Identification of enriched transcription factor motifs

After linking the snRNA-seq and snATAC-seq data, we performed the enriched transcription factors motif analysis with Signac based on the linked snRNA-ATAC-seq data. A list of motif position frequency matrices from the JASPAR database was obtained and the reference motif information *BSgenome.Hsapiens.UCSC.hg38* was added to the Seurat object using the *AddMotifs* function. Enriched motifs of all differentially expressed genes of individual cell type between Control and Fontan were analyzed using the *FindMotifs* function with the default setting.

Identification of ligand-receptor interactions

We identified ligand-receptor interaction between all 7 cell types using CellChat (46). Normalized and harmonized Fontan gene-by-cell expression matrix (16,047 nuclei) was used as the input. The *CellChatDB.human* was used as our reference database. We preprocessed the expression data by identifying over-expressed ligands or receptors in one cell group and then overexpressed ligand-receptor interactions using *identifyOverExpressedGenes* and *identifyOverExpressedInteractions* in CellChat. The truncated mean value was set to 5% and the ligand-receptor pair communication probability was then analyzed using *computeCommunProbPathway* and all communication networks were aggregated using the *aggregateNet* function in CellChat with the default setting.

Cell culture

MRC-5 human fibroblast cells (ATCC CCL-171) were cultured in DMEM with 10% FBS (Gemini) and 1x antibiotic-antimycotic (ThermoFisher 15240062). Cells were plated and then starved overnight in 1% FBS. PBS (negative control), 10 ng/ml TGFβ (Peprotech 100-21, as positive control), 10, 30, or 100 ng/ml of Activin A (Peprotech 120-14P), Activin

B (R&D 659-AB-005) or Activin C (R&D 1629-AC-010) were then added to MRC-5 cells for 72 hours. Each treatment was performed in biological triplicate.

RNA and protein analysis

We isolated total RNA from MRC-5 cells using RNAzol RT (Molecular Research Center) following the manufacturer's instructions. Control and Fontan cDNA were obtained from snRNA-ATAC-seq library preparation step. We performed qRT-PCR, immunohistochemistry and Western Blot as previously described (47–51). We ran qPCR in technical triplicates and calculated relative mRNA abundance using a standard curve and normalized to *36B4* mRNA abundance in the same sample. qPCR primers used are: ACTA2: GTGTTGCCCCTGAAGAGCAT & GCTGGGACATTGAAAGTCTCA; COL4A1: GGGATGCTGTTGAAAGGTGAA & GGTGGTCCGGTAAATCCTGG; ACOX2: CTGATGCTTTTGACTTCACCG & GGGTTCTCCTGAGTATTGGTTG; ADH1C: AGAGTATCCGTACCGTCCTG & TCCAGATCATGTAGGGTAGAGG; CAT: GTACATTTAATACAGCAGTGTCATCAG & TTGATCTGTTGTGAAATCAGTGC; COL6A1: CTCAAGACCCTCGAGATTAACG & GGAAGGAGAGGTTTGCGTTG; COL4A4: TGCAGATGTGGATGACTGTC & AGCATCAAACATAGCGAGAGG; 36B4: CAGATTGGCTACCCAACTGTT & GGGAAGGTGTAATCCGTCTCC. For Western Blot, we isolated total protein from MRC-5 using Glo Lysis Buffer (Promega) with Protease Inhibitor added (Roche) following the manufacturer's instructions. We ran Western Blot with biological duplicates and normalized to βACTIN in the same sample. Catalase antibody for immunohistochemistry is from Abcam (ab16731). ACTA2 antibody for Western Blot is from Novius (SY02-64). βACTIN antibody for Western Blot is from Proteintech (66999-1-Ig).

Plasmid Construction

The human NRF1 and ZNF148 plasmids were gifts from Feng Zhang (Addgene plasmid #142523, http://n2t.net/addgene:142523, RRID:Addgene_142523; and Addgene plasmid #141822; http://n2t.net/addgene:141822, RRID: Addgene_141822) (52). The reporter plasmid PGL4.23-*INHBA* was constructed by inserting human *INHBA* promoter sequence chr7-41705382-41705772 into the pGL4.23 vector (Promega).

Luciferase Reporter Assay

HEK293T cells were cultured in DMEM with 10% FBS (Gemini) and 1x antibiotic-antimycotic (ThermoFisher 15240062). Cells were plated 24h before transfection in black 24-well plate (ibidi) at 0.1×10^6 cells/well. Each well of cells was transfected with 450ng of transcription factor plasmids (empty-vector, NRF1, ZNF148, PPARα, and PPARγ), 150ng of reporter plasmid (PGL4.23-empty, PGL4.23-*INHBA*), and 15ng of Renilla plasmid (Promega) using PEI MAX Transfection reagent (Polysciences) following the manufacturer's instructions. Each group was performed in biological triplicates. Luciferase activity was measured 48 hours after transfection using the Dual-Glo Luciferase Assay System (Promega) following the manufacturer's instructions. Firefly luciferase activity was normalized to Renilla luciferase activity.

Statistical analysis

Non-parametric Wilcoxon Rank Sum test, likelihood ratio test, and two-sample unequal variance Student's t-test were performed in R or Microsoft Excel to determine statistical significance, with a $p<0.05$ deemed as statistically significant.

Supplementary Material

Refer to Web version on PubMed Central for supplementary material.

Acknowledgments:

We are grateful to the CHOP Fred & Suzanne Biesecker Liver Center Tissue Repository for providing us the control liver samples. We thank Dr. Matthew D. Weitzman for the MRC-5 cells. We thank Lu Gan, Peiran Lu, Ting Peng, Riley Sawka, Ghita Benjelloun, Anusha Thaliana, Liya Mooradian, Changya Chen and Shiping Zhang for assistance.

Funding:

This work and the authors are supported by the Office of the Assistant Secretary of Defense for Health Affairs through the Peer Reviewed Medical Research Program under Awards W81XWH20-1-0042, W81XWH20-1-0089, W81XWH22-1-0058 and W81XWH22-1-0561, NIH R01DK111495, U54HL165442, U01HL166058, P30DK019525, American Heart Association Established Investigator Award 227477, CHOP Foerderer Award, an SVRF grant from Additional Ventures (P.H., J.Z., H.B., A.B. and L.P.), and by the Robert & Dolores Harrington Endowed Chair in Cardiology at the Children's Hospital of Philadelphia (J.R.).

Data and materials availability:

Raw and processed snRNA-ATAC-seq data are deposited in the GEO database (GSE223843). All other data associated with this study are in the paper or the Supplementary Materials.

References and Notes

1. Schilling C, Dalziel K, Nunn R, Du Plessis K, Shi WY, Celermajer D, Winlaw D, Weintraub RG, Grigg LE, Radford DJ, Bullock A, Gentles TL, Wheaton GR, Hornung T, Justo RN, d'Udekem Y, The Fontan epidemic: Population projections from the Australia and New Zealand Fontan Registry. Int J Cardiol 219, 14–19 (2016). [PubMed: 27257850]
2. Rychik J, Atz AM, Celermajer DS, Deal BJ, Gatzoulis MA, Gewillig MH, Hsia TY, Hsu DT, Kovacs AH, McCrindle BW, Newburger JW, Pike NA, Rodefeld M, Rosenthal DN, Schumacher KR, Marino BS, Stout K, Veldtman G, Younoszai AK, d'Udekem Y, American Heart Association Council on Cardiovascular Disease in the, C. Council on, N. Stroke, Evaluation and Management of the Child and Adult With Fontan Circulation: A Scientific Statement From the American Heart Association. Circulation, CIR0000000000000696 (2019).
3. Goldberg DJ, Surrey LF, Glatz AC, Dodds K, O'Byrne ML, Lin HC, Fogel M, Rome JJ, Rand EB, Russo P, Rychik J, Hepatic Fibrosis Is Universal Following Fontan Operation, and Severity is Associated With Time From Surgery: A Liver Biopsy and Hemodynamic Study. J Am Heart Assoc 6, (2017).
4. Rychik J, Forty years of the Fontan operation: a failed strategy. Semin Thorac Cardiovasc Surg Pediatr Card Surg Annu 13, 96–100 (2010). [PubMed: 20307870]
5. Dennis M, Zannino D, du Plessis K, Bullock A, Disney PJS, Radford DJ, Hornung T, Grigg L, Cordina R, d'Udekem Y, Celermajer DS, Clinical Outcomes in Adolescents and Adults After the Fontan Procedure. J Am Coll Cardiol 71, 1009–1017 (2018). [PubMed: 29495980]
6. Rychik J, Kim Y, The Adolescent and Adult With a Fontan Circulation: "Unnatural" Selection and Survival of the Fittest. J Am Coll Cardiol 71, 1018–1020 (2018). [PubMed: 29495981]

7. Malhi H, Brown RS Jr., Lim JK, Reau N, Tapper EB, Wong CC, Gores GJ, Precipitous changes in nomenclature and definitions-NAFLD becomes SLD: Implications for and expectations of AASLD journals. Hepatol Commun 7, (2023).
8. Tanay A, Regev A, Scaling single-cell genomics from phenomenology to mechanism. Nature 541, 331–338 (2017). [PubMed: 28102262]
9. Tabula Muris Consortium, Single-cell transcriptomics of 20 mouse organs creates a Tabula Muris. Nature 562, 367–372 (2018). [PubMed: 30283141]
10. Cusanovich DA, Hill AJ, Aghamirzaie D, Daza RM, Pliner HA, Berletch JB, Filippova GN, Huang X, Christiansen L, DeWitt WS, Lee C, Regalado SG, Read DF, Steemers FJ, Disteche CM, Trapnell C, Shendure J, A Single-Cell Atlas of In Vivo Mammalian Chromatin Accessibility. Cell 174, 1309–1324 e1318 (2018). [PubMed: 30078704]
11. Eraslan G, Drokhlyansky E, Anand S, Fiskin E, Subramanian A, Slyper M, Wang J, Van Wittenberghe N, Rouhana JM, Waldman J, Ashenberg O, Lek M, Dionne D, Win TS, Cuoco MS, Kuksenko O, Tsankov AM, Branton PA, Marshall JL, Greka A, Getz G, Segre AV, Aguet F, Rozenblatt-Rosen O, Ardlie KG, Regev A, Single-nucleus cross-tissue molecular reference maps toward understanding disease gene function. Science 376, eabl4290 (2022). [PubMed: 35549429]
12. Tabula Sapiens C, Jones RC, Karkanias J, Krasnow MA, Pisco AO, Quake SR, Salzman J, Yosef N, Bulthaup B, Brown P, Harper W, Hemenez M, Ponnusamy R, Salehi A, Sanagavarapu BA, Spallino E, Aaron KA, Concepcion W, Gardner JM, Kelly B, Neidlinger N, Wang Z, Crasta S, Kolluru S, Morri M, Pisco AO, Tan SY, Travaglini KJ, Xu C, Alcantara-Hernandez M, Almanzar N, Antony J, Beyersdorf B, Burhan D, Calcuttawala K, Carter MM, Chan CKF, Chang CA, Chang S, Colville A, Crasta S, Culver RN, Cvijovic I, D'Amato G, Ezran C, Galdos FX, Gillich A, Goodyer WR, Hang Y, Hayashi A, Houshdaran S, Huang X, Irwin JC, Jang S, Juanico JV, Kershner AM, Kim S, Kiss B, Kolluru S, Kong W, Kumar ME, Kuo AH, Leylek R, Li B, Loeb GB, Lu WJ, Mantri S, Markovic M, McAlpine PL, de Morree A, Morri M, Mrouj K, Mukherjee S, Muser T, Neuhofer P, Nguyen TD, Perez K, Phansalkar R, Pisco AO, Puluca N, Qi Z, Rao P, Raquer-McKay H, Schaum N, Scott B, Seddighzadeh B, Segal J, Sen S, Sikandar S, Spencer SP, Steffes LC, Subramaniam VR, Swarup A, Swift M, Travaglini KJ, Van Treuren W, Trimm E, Veizades S, Vijayakumar S, Vo KC, Vorperian SK, Wang W, Weinstein HNW, Winkler J, Wu TTH, Xie J, Yung AR, Zhang Y, Detweiler AM, Mekonen H, Neff NF, Sit RV, Tan M, Yan J, Bean GR, Charu V, Forgo E, Martin BA, Ozawa MG, Silva O, Tan SY, Toland A, Vemuri VNP, Afik S, Awayan K, Botvinnik OB, Byrne A, Chen M, Dehghannasiri R, Detweiler AM, Gayoso A, Granados AA, Li Q, Mahmoudabadi G, McGeever A, de Morree A, Olivieri JE, Park M, Pisco AO, Ravikumar N, Salzman J, Stanley G, Swift M, Tan M, Tan W, Tarashansky AJ, Vanheusden R, Vorperian SK, Wang P, Wang S, Xing G, Xu C, Yosef N, Alcantara-Hernandez M, Antony J, Chan CKF, Chang CA, Colville A, Crasta S, Culver R, Dethlefsen L, Ezran C, Gillich A, Hang Y, Ho PY, Irwin JC, Jang S, Kershner AM, Kong W, Kumar ME, Kuo AH, Leylek R, Liu S, Loeb GB, Lu WJ, Maltzman JS, Metzger RJ, de Morree A, Neuhofer P, Perez K, Phansalkar R, Qi Z, Rao P, Raquer-McKay H, Sasagawa K, Scott B, Sinha R, Song H, Spencer SP, Swarup A, Swift M, Travaglini KJ, Trimm E, Veizades S, Vijayakumar S, Wang B, Wang W, Winkler J, Xie J, Yung AR, Artandi SE, Beachy PA, Clarke MF, Giudice LC, Huang FW, Huang KC, Idoyaga J, Kim SK, Krasnow M, Kuo CS, Nguyen P, Quake SR, Rando TA, Red-Horse K, Reiter J, Relman DA, Sonnenburg JL, Wang B, Wu A, Wu SM, Wyss-Coray T, The Tabula Sapiens: A multiple-organ, single-cell transcriptomic atlas of humans. Science 376, eabl4896 (2022). [PubMed: 35549404]
13. Argelaguet R, Cuomo ASE, Stegle O, Marioni JC, Computational principles and challenges in single-cell data integration. Nat Biotechnol 39, 1202–1215 (2021). [PubMed: 33941931]
14. Luecken MD, Buttner M, Chaichoompu K, Danese A, Interlandi M, Mueller MF, Strobl DC, Zappia L, Dugas M, Colome-Tatche M, Theis FJ, Benchmarking atlas-level data integration in single-cell genomics. Nat Methods 19, 41–50 (2022). [PubMed: 34949812]
15. Korsunsky I, Millard N, Fan J, Slowikowski K, Zhang F, Wei K, Baglaenko Y, Brenner M, Loh PR, Raychaudhuri S, Fast, sensitive and accurate integration of single-cell data with Harmony. Nat Methods 16, 1289–1296 (2019). [PubMed: 31740819]
16. Matsusue K, Haluzik M, Lambert G, Yim SH, Gavrilova O, Ward JM, Brewer B Jr., Reitman ML, Gonzalez FJ, Liver-specific disruption of PPARgamma in leptin-deficient mice improves fatty liver but aggravates diabetic phenotypes. J Clin Invest 111, 737–747 (2003). [PubMed: 12618528]

17. Gavrilova O, Haluzik M, Matsusue K, Cutson JJ, Johnson L, Dietz KR, Nicol CJ, Vinson C, Gonzalez FJ, Reitman ML, Liver peroxisome proliferator-activated receptor gamma contributes to hepatic steatosis, triglyceride clearance, and regulation of body fat mass. J Biol Chem 278, 34268–34276 (2003). [PubMed: 12805374]
18. Moran-Salvador E, Lopez-Parra M, Garcia-Alonso V, Titos E, Martinez-Clemente M, Gonzalez-Periz A, Lopez-Vicario C, Barak Y, Arroyo V, Claria J, Role for PPARgamma in obesity-induced hepatic steatosis as determined by hepatocyte- and macrophage-specific conditional knockouts. Faseb J 25, 2538–2550 (2011). [PubMed: 21507897]
19. Lin SJ, Zhang Y, Liu NC, Yang DR, Li G, Chang C, Minireview: Pathophysiological roles of the TR4 nuclear receptor: lessons learned from mice lacking TR4. Mol Endocrinol 28, 805–821 (2014). [PubMed: 24702179]
20. Kang HS, Okamoto K, Kim YS, Takeda Y, Bortner CD, Dang H, Wada T, Xie W, Yang XP, Liao G, Jetten AM, Nuclear orphan receptor TAK1/TR4-deficient mice are protected against obesity-linked inflammation, hepatic steatosis, and insulin resistance. Diabetes 60, 177–188 (2011). [PubMed: 20864514]
21. Satoh J, Kawana N, Yamamoto Y, Pathway Analysis of ChIP-Seq-Based NRF1 Target Genes Suggests a Logical Hypothesis of their Involvement in the Pathogenesis of Neurodegenerative Diseases. Gene Regul Syst Bio 7, 139–152 (2013).
22. Consortium EP, An integrated encyclopedia of DNA elements in the human genome. Nature 489, 57–74 (2012). [PubMed: 22955616]
23. Xiong X, Kuang H, Ansari S, Liu T, Gong J, Wang S, Zhao XY, Ji Y, Li C, Guo L, Zhou L, Chen Z, Leon-Mimila P, Chung MT, Kurabayashi K, Opp J, Campos-Perez F, Villamil-Ramirez H, Canizales-Quinteros S, Lyons R, Lumeng CN, Zhou B, Qi L, Huertas-Vazquez A, Lusis AJ, Xu XZS, Li S, Yu Y, Li JZ, Lin JD, Landscape of Intercellular Crosstalk in Healthy and NASH Liver Revealed by Single-Cell Secretome Gene Analysis. Mol Cell 75, 644–660 e645 (2019). [PubMed: 31398325]
24. Barrow F, Khan S, Fredrickson G, Wang H, Dietsche K, Parthiban P, Robert S, Kaiser T, Winer S, Herman A, Adeyi O, Mouzaki M, Khoruts A, Hogquist KA, Staley C, Winer DA, Revelo XS, Microbiota-Driven Activation of Intrahepatic B Cells Aggravates NASH Through Innate and Adaptive Signaling. Hepatology 74, 704–722 (2021). [PubMed: 33609303]
25. Peiseler M, Schwabe R, Hampe J, Kubes P, Heikenwalder M, Tacke F, Immune mechanisms linking metabolic injury to inflammation and fibrosis in fatty liver disease - novel insights into cellular communication circuits. J Hepatol 77, 1136–1160 (2022). [PubMed: 35750137]
26. Fred RG, Steen Pedersen J, Thompson JJ, Lee J, Timshel PN, Stender S, Opseth Rygg M, Gluud LL, Bjerregaard Kristiansen V, Bendtsen F, Hansen T, Pers TH, Single-cell transcriptome and cell type-specific molecular pathways of human non-alcoholic steatohepatitis. Sci Rep 12, 13484 (2022). [PubMed: 35931712]
27. Wang S, Li K, Pickholz E, Dobie R, Matchett KP, Henderson NC, Carrico C, Driver I, Borch Jensen M, Chen L, Petitjean M, Bhattacharya D, Fiel MI, Liu X, Kisseleva T, Alon U, Adler M, Medzhitov R, Friedman SL, An autocrine signaling circuit in hepatic stellate cells underlies advanced fibrosis in nonalcoholic steatohepatitis. Sci Transl Med 15, eadd3949 (2023). [PubMed: 36599008]
28. O'Connell TM, Logsdon DL, Mitscher G, Payne RM, Metabolic profiles identify circulating biomarkers associated with heart failure in young single ventricle patients. Metabolomics 17, 95 (2021). [PubMed: 34601638]
29. Michel M, Dubowy KO, Entenmann A, Karall D, Adam MG, Zlamy M, Odri Komazec I, Geiger R, Niederwanger C, Salvador C, Muller U, Laser KT, Scholl-Burgi S, Targeted metabolomic analysis of serum amino acids in the adult Fontan patient with a dominant left ventricle. Sci Rep 10, 8930 (2020). [PubMed: 32488174]
30. Michel M, Dubowy KO, Zlamy M, Karall D, Adam MG, Entenmann A, Keller MA, Koch J, Odri Komazec I, Geiger R, Salvador C, Niederwanger C, Muller U, Scholl-Burgi S, Laser KT, Targeted metabolomic analysis of serum phospholipid and acylcarnitine in the adult Fontan patient with a dominant left ventricle. Ther Adv Chronic Dis 11, 2040622320916031 (2020). [PubMed: 32426103]

31. Sonoda J, Pei L, Evans RM, Nuclear receptors: decoding metabolic disease. FEBS Lett 582, 2–9 (2008). [PubMed: 18023286]
32. Skat-Rordam J, Hojland Ipsen D, Lykkesfeldt J, Tveden-Nyborg P, A role of peroxisome proliferator-activated receptor gamma in non-alcoholic fatty liver disease. Basic Clin Pharmacol Toxicol 124, 528–537 (2019). [PubMed: 30561132]
33. Gong L, Wei F, Gonzalez FJ, Li G, Hepatic fibrosis: targeting peroxisome proliferator-activated receptor alpha from mechanism to medicines. Hepatology, (2023).
34. Francque SM, Bedossa P, Ratziu V, Anstee QM, Bugianesi E, Sanyal AJ, Loomba R, Harrison SA, Balabanska R, Mateva L, Lanthier N, Alkhouri N, Moreno C, Schattenberg JM, Stefanova-Petrova D, Vonghia L, Rouzier R, Guillaume M, Hodge A, Romero-Gomez M, Huot-Marchand P, Baudin M, Richard MP, Abitbol JL, Broqua P, Junien JL, Abdelmalek MF, Group NS, A Randomized, Controlled Trial of the Pan-PPAR Agonist Lanifibranor in NASH. N Engl J Med 385, 1547–1558 (2021). [PubMed: 34670042]
35. Scarpulla RC, Nuclear control of respiratory gene expression in mammalian cells. J Cell Biochem 97, 673–683 (2006). [PubMed: 16329141]
36. Jornayvaz FR, Shulman GI, Regulation of mitochondrial biogenesis. Essays Biochem 47, 69–84 (2010). [PubMed: 20533901]
37. Chen T, Oh S, Gregory S, Shen X, Diehl AM, Single-cell omics analysis reveals functional diversification of hepatocytes during liver regeneration. JCI Insight 5, (2020).
38. Kang B, Kang B, Roh TY, Seong RH, Kim W, The Chromatin Accessibility Landscape of Nonalcoholic Fatty Liver Disease Progression. Mol Cells 45, 343–352 (2022). [PubMed: 35422452]
39. Wang Y, Hamang M, Culver A, Jiang H, Yanum J, Garcia V, Lee J, White E, Kusumanchi P, Chalasani N, Liangpunsakul S, Yaden BC, Dai G, Activin B promotes the initiation and progression of liver fibrosis. Hepatol Commun 6, 2812–2826 (2022). [PubMed: 35866567]
40. Kiagiadaki F, Kampa M, Voumvouraki A, Castanas E, Kouroumalis E, Notas G, Activin-A causes Hepatic stellate cell activation via the induction of TNFalpha and TGFbeta in Kupffer cells. Biochim Biophys Acta Mol Basis Dis 1864, 891–899 (2018). [PubMed: 29287776]
41. Rychik J, Veldtman G, Rand E, Russo P, Rome JJ, Krok K, Goldberg DJ, Cahill AM, Wells RG, The precarious state of the liver after a Fontan operation: summary of a multidisciplinary symposium. Pediatr Cardiol 33, 1001–1012 (2012). [PubMed: 22534759]
42. Rychik J, Goldberg DJ, Rand E, Mancilla EE, Heimall J, Seivert N, Campbell D, O'Malley S, Dodds KM, A Path FORWARD: Development of a Comprehensive Multidisciplinary Clinic to Create Health and Wellness for the Child and Adolescent with a Fontan Circulation. Pediatr Cardiol 43, 1175–1192 (2022). [PubMed: 35604474]
43. Yu W, Uzun Y, Zhu Q, Chen C, Tan K, scATAC-pro: a comprehensive workbench for single-cell chromatin accessibility sequencing data. Genome Biol 21, 94 (2020). [PubMed: 32312293]
44. Hu P, Liu J, Zhao J, Wilkins BJ, Lupino K, Wu H, Pei L, Single-nucleus transcriptomic survey of cell diversity and functional maturation in postnatal mammalian hearts. Genes Dev 32, 1344–1357 (2018). [PubMed: 30254108]
45. Stuart T, Srivastava A, Madad S, Lareau CA, Satija R, Single-cell chromatin state analysis with Signac. Nat Methods 18, 1333–1341 (2021). [PubMed: 34725479]
46. Jin S, Guerrero-Juarez CF, Zhang L, Chang I, Ramos R, Kuan CH, Myung P, Plikus MV, Nie Q, Inference and analysis of cell-cell communication using CellChat. Nat Commun 12, 1088 (2021). [PubMed: 33597522]
47. Wang T, McDonald C, Petrenko NB, Leblanc M, Giguere V, Evans RM, Patel VV, Pei L, Estrogen-related receptor alpha (ERRalpha) and ERRgamma are essential coordinators of cardiac metabolism and function. Mol Cell Biol 35, 1281–1298 (2015). [PubMed: 25624346]
48. Pei L, Mu Y, Leblanc M, Alaynick W, Barish GD, Pankratz M, Tseng TW, Kaufman S, Liddle C, Yu RT, Downes M, Pfaff SL, Auwerx J, Gage FH, Evans RM, Dependence of Hippocampal Function on ERRgamma-Regulated Mitochondrial Metabolism. Cell Metab 21, 628–636 (2015). [PubMed: 25863252]

49. Wang T, Liu J, McDonald C, Lupino K, Zhai X, Wilkins BJ, Hakonarson H, Pei L, GDF15 is a heart-derived hormone that regulates body growth. EMBO Mol Med 9, 1150–1164 (2017). [PubMed: 28572090]

50. Li JJ, Liu J, Lupino K, Liu X, Zhang L, Pei L, Growth Differentiation Factor 15 Maturation Requires Proteolytic Cleavage by PCSK3, -5, and -6. Mol Cell Biol 38, (2018).

51. Zhao J, Lupino K, Wilkins BJ, Qiu C, Liu J, Omura Y, Allred AL, McDonald C, Susztak K, Barish GD, Pei L, Genomic integration of ERRgamma-HNF1beta regulates renal bioenergetics and prevents chronic kidney disease. Proc Natl Acad Sci U S A 115, E4910–E4919 (2018). [PubMed: 29735694]

52. Joung J, Ma S, Tay T, Geiger-Schuller KR, Kirchgatterer PC, Verdine VK, Guo B, Arias-Garcia MA, Allen WE, Singh A, Kuksenko O, Abudayyeh OO, Gootenberg JS, Fu Z, Macrae RK, Buenrostro JD, Regev A, Zhang F, A transcription factor atlas of directed differentiation. Cell 186, 209–229 e226 (2023). [PubMed: 36608654]

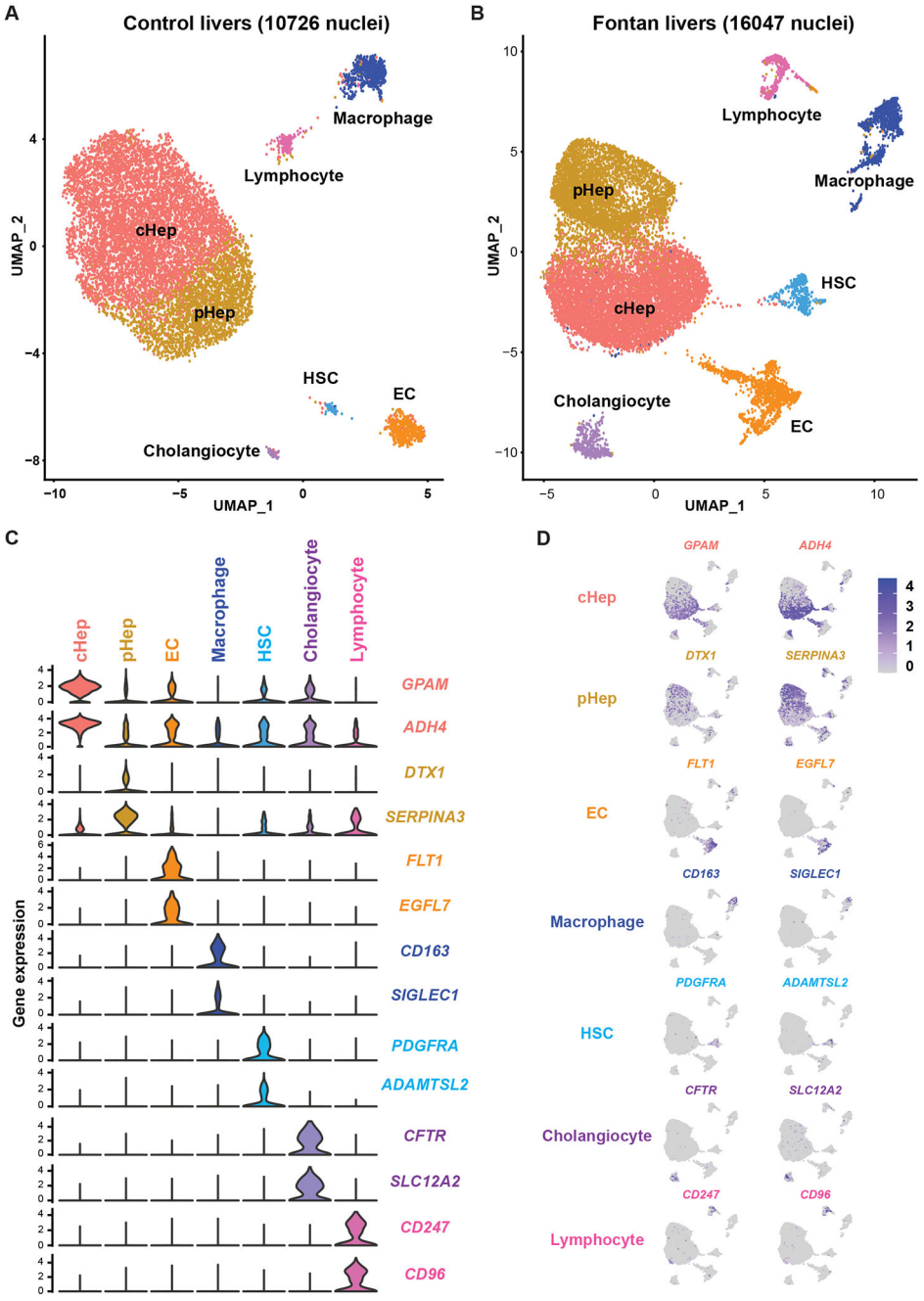

Fig. 1. The single-cell transcriptomic atlas of human FALD.

(**A and B**) UMAP of the snRNA-ATAC-seq transcriptome data of the control (A, n=2) and FC (B, n=4) livers. The total numbers of high-quality nuclei containing both the transcriptome and epigenome data are labeled, as are transcriptome-based cellular identities. (**C and D**) Violin plots (C) and feature plots (D) illustrating cluster-specific marker gene expression of each cell type in the FC livers (log_2[fold change]>0.25 and percentage of positive cells>25%).

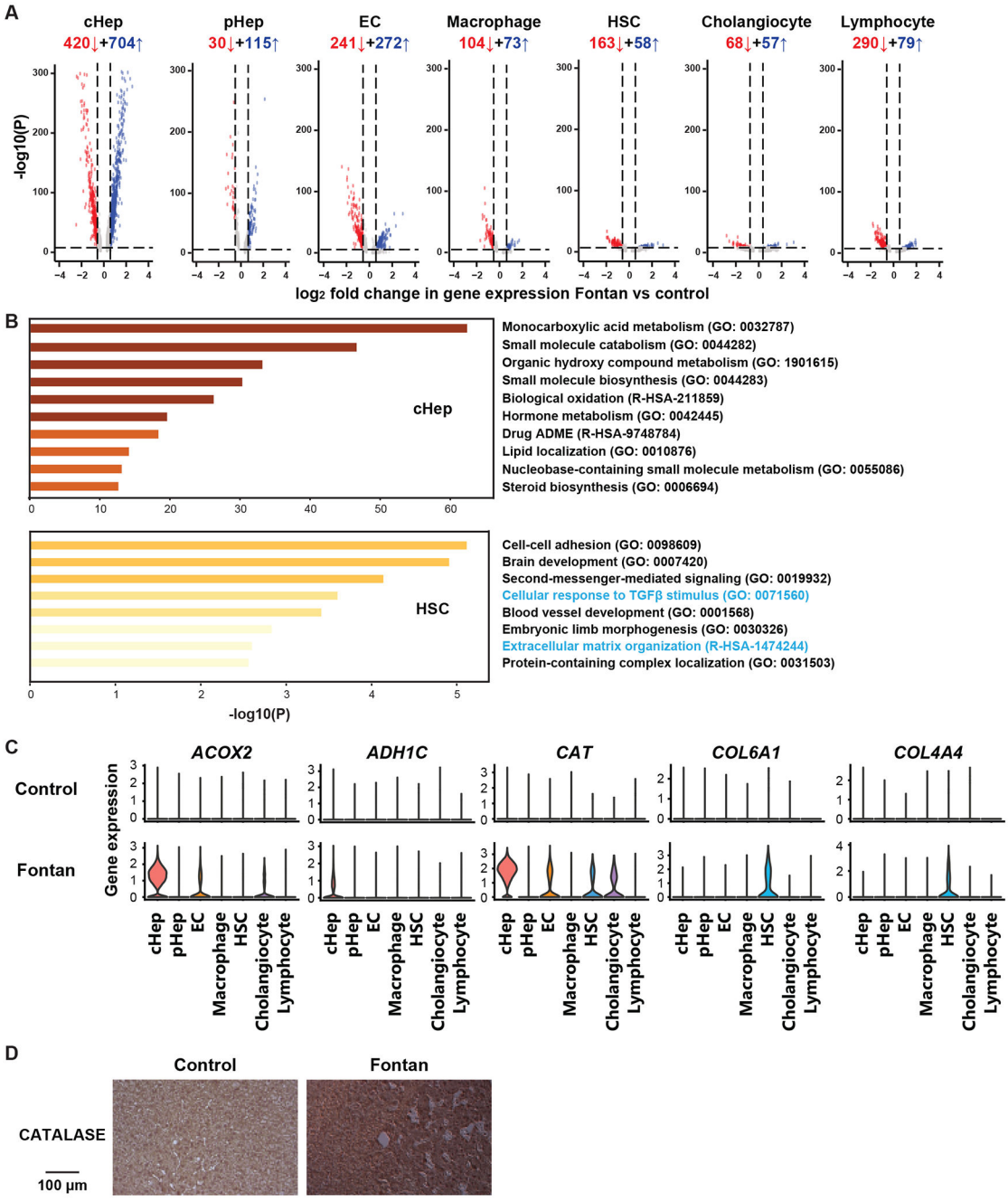

Fig. 2. Cell type-specific liver transcriptional remodeling in human FALD.

(**A**) Volcano plots showing differentially expressed genes (DEGs) in correlated cell types of control (n= 2) and FC (n= 4) livers. Numbers of upregulated (blue) and downregulated (red) genes in the FC livers are labeled. (**B**) Enriched pathways of genes significantly upregulated in central hepatocytes (cHeps) and hepatic stellate cells (HSCs) of FC livers by gene ontology (GO) analysis. (**C**) Violin plots showing representative genes significantly ($P<1x10^{-5}$ and $\log_2$[fold change]>0.58) upregulated in cHeps and HSCs of FC livers. (**D**) Immunohistochemistry of Catalase using control and FC liver sections.

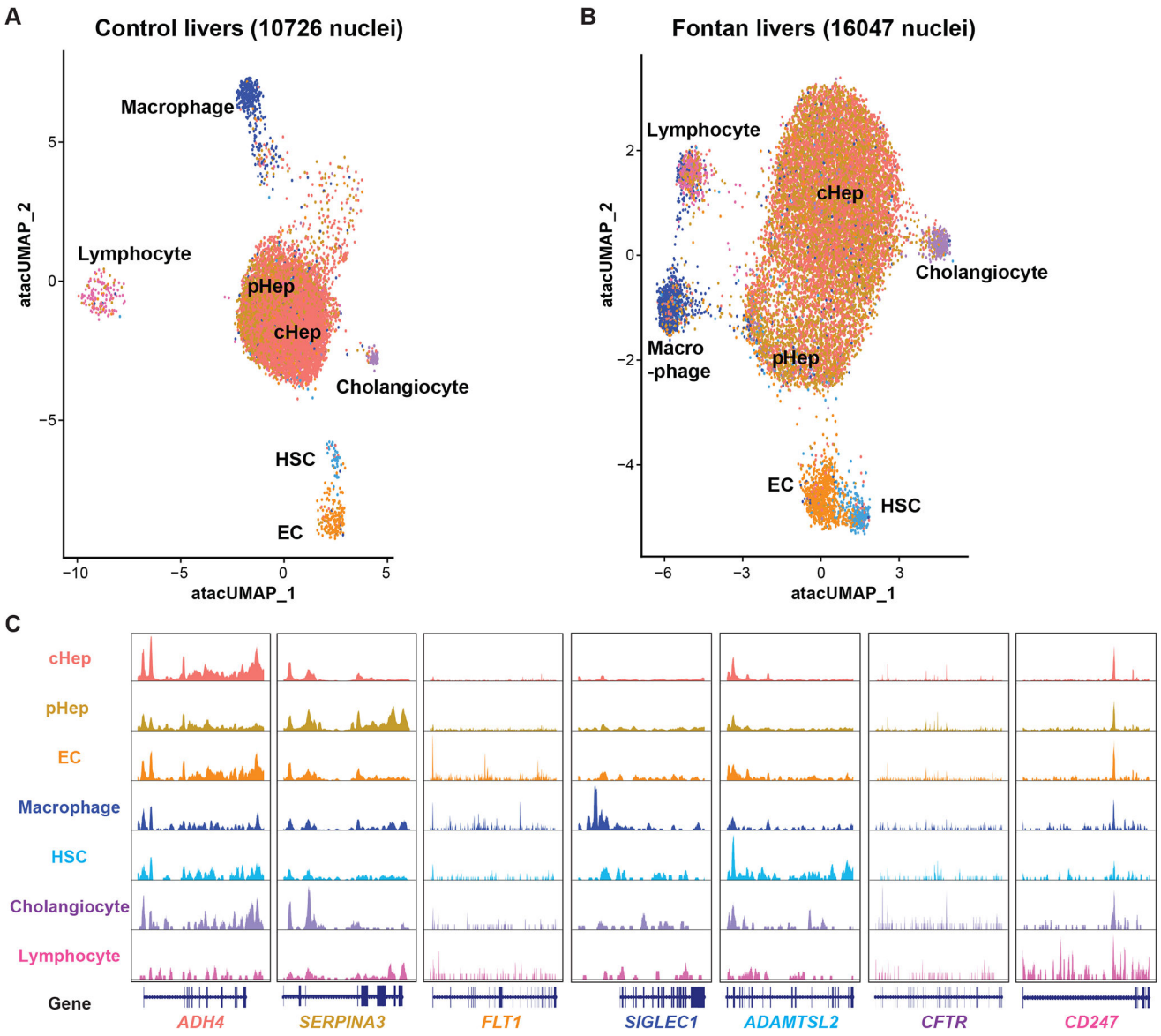

Fig. 3. The single-cell liver epigenomic atlas of human FALD.

(**A and B**) UMAP of the snRNA-ATAC-seq epigenome data of the control (A, n=2) and FC (B, n=4) livers. Cell identities based on their epigenomes and linked transcriptomes are labeled. (**C**) Aggregated ATAC signal (peaks) of representative cell type-specific genes in each cell type of FC livers. The gene structures are shown at the bottom, all with 5' on the left.

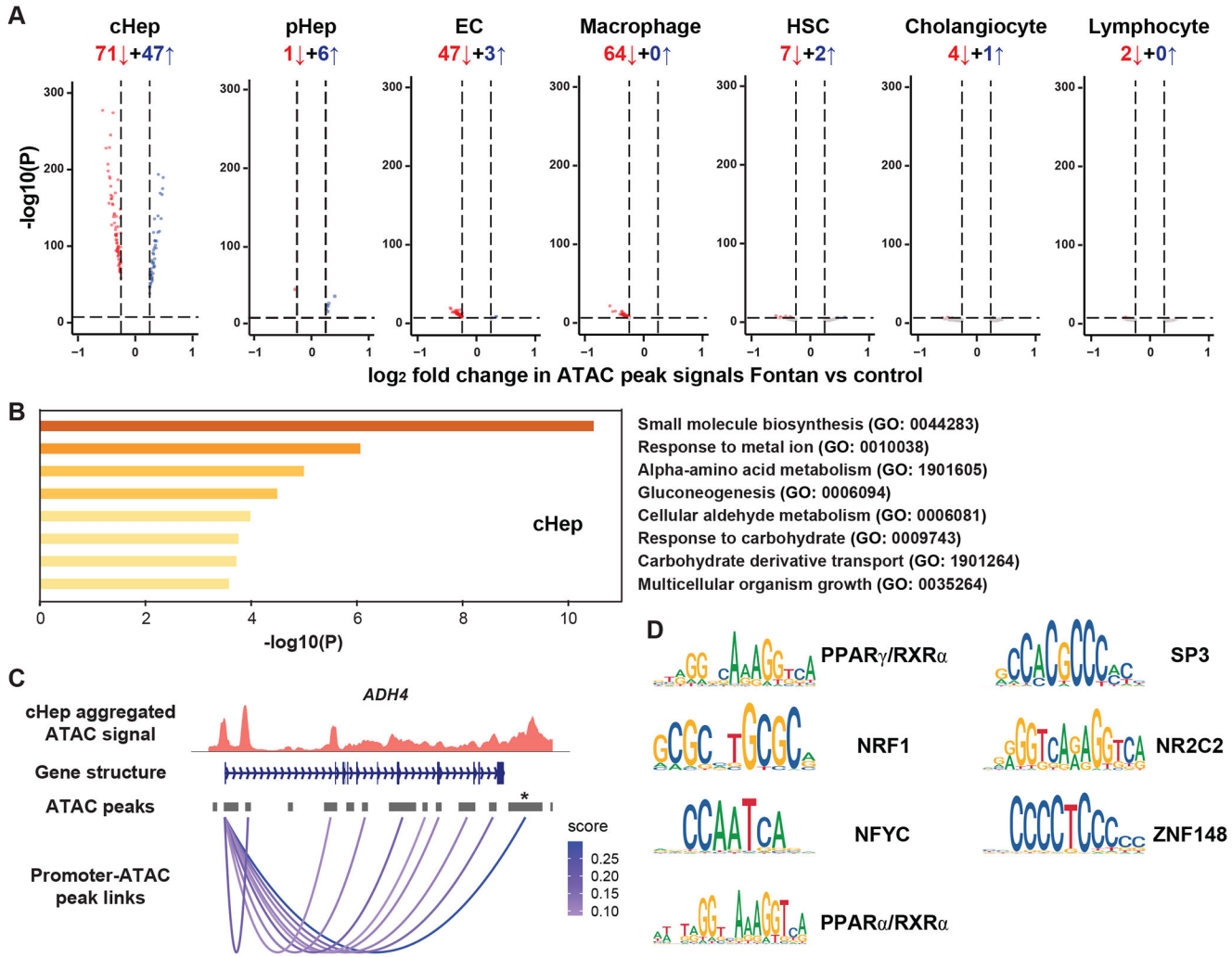

Fig. 4. Cell type-specific liver epigenetic remodeling in human FALD.

(**A**) Volcano plots showing differential ATAC peaks in correlated cell types of control (n=2) and FC (n=4) livers. Numbers of upregulated (blue) and downregulated (red) ATAC peaks in the FC livers are labeled. (**B**) Enriched pathways of genes linked to ATAC peaks more accessible in FC cHeps by gene ontology (GO) analysis. (**C**) Single-cell level joint gene expression and chromatin accessibility analysis uncovering chromatin regions important for *ADH4* gene expression. The higher the score, the stronger correlation between each linked chromatin region and *ADH4* expression. (**D**) Enriched DNA sequence motifs ($P<6.3x10^{-20}$ and log_2[fold enrichment]>1.35) and associated transcription factors of chromatin regions linked to increased metabolic gene expression in cHeps.

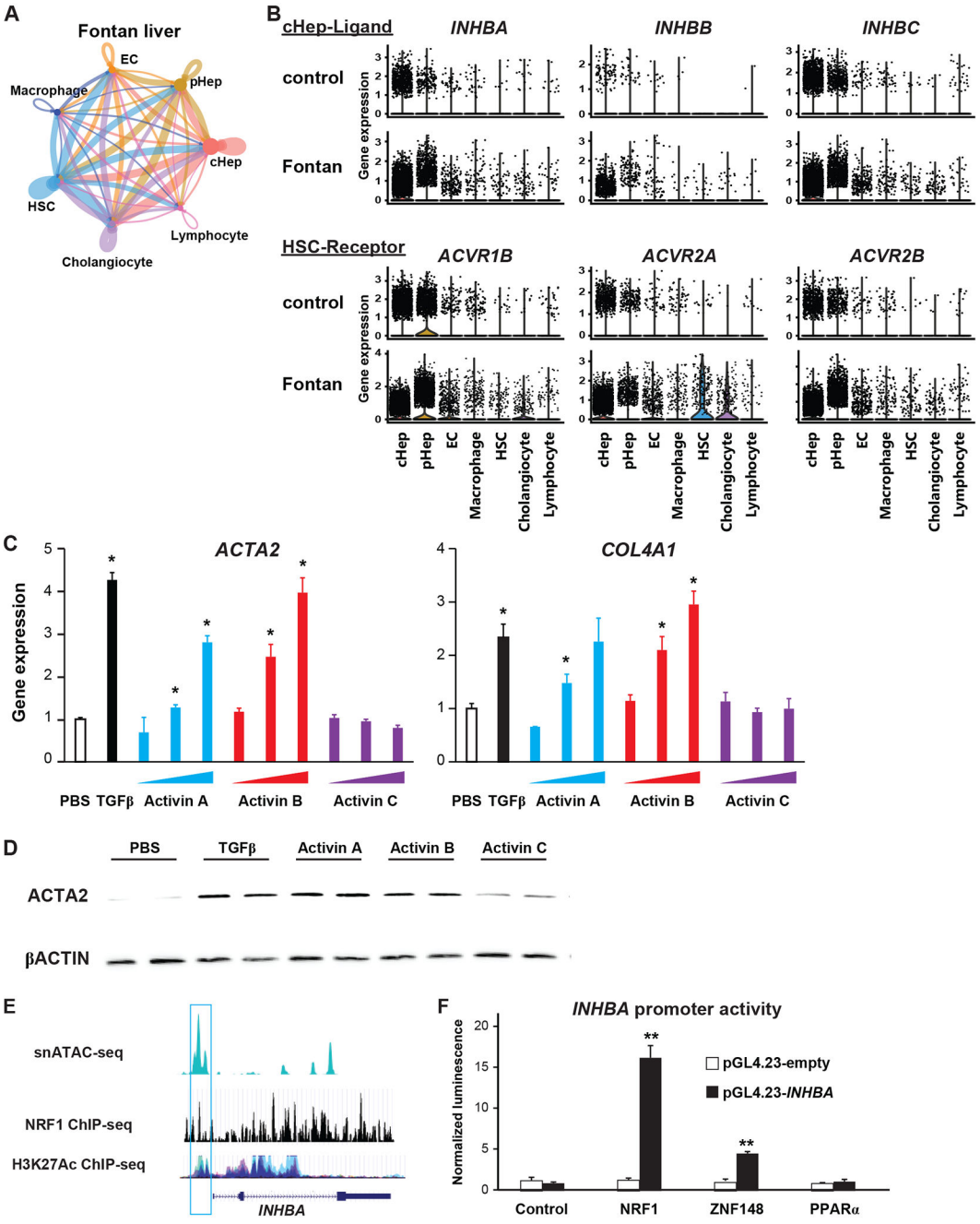

Fig. 5. cHep to HSC signaling promotes HSC activation and liver fibrosis in FALD.

(**A**) Ligand-receptor pairs in FALD revealed by snRNA-ATAC-seq data. The bigger the circle and the thicker the line, the more ligand-receptor pairs included. (**B**) Violin plots showing gene expression of ligands *INHBA*, *INHBB*, *INHBC* and receptors *ACVR1B*, *ACVR2A*, and *ACVR2B* in different cell types of control (n=2) and FC (n=4) livers. (**C**) *ACTA2* and *COL4A1* expression by qPCR in MRC-5 cells treated with PBS (as control), 10ng/ml TGFβ, and 10, 30, and 100 ng/ml of Activin A, B, or C for 72 hours. n=3 biological replicates for each treatment. Error bars are standard error of the mean. *p<0.05 vs control.

(**D**) ACTA2 and βACTIN (as loading control) protein abundance in MRC-5 cells treated with PBS, 10ng/ml TGFβ, or 100 ng/ml of Activin A, B or C for 72 hours. (**E**) Alignment of aggregated FALD snATAC-seq (this study), published NRF1 ChIP-seq (21), and H3K27Ac ChIP-seq (22) signals showing that an accessible region in the promoter of human INHBA gene is bound by NRF1 and H3K27 in this region is acetylated. (**F**) NRF1 and ZNF148 but not PPARα activate *INHBA* promoter in a luciferase reporter assay (n=3 biological replicates). Error bars are standard error of the mean. **p<0.01 vs control.

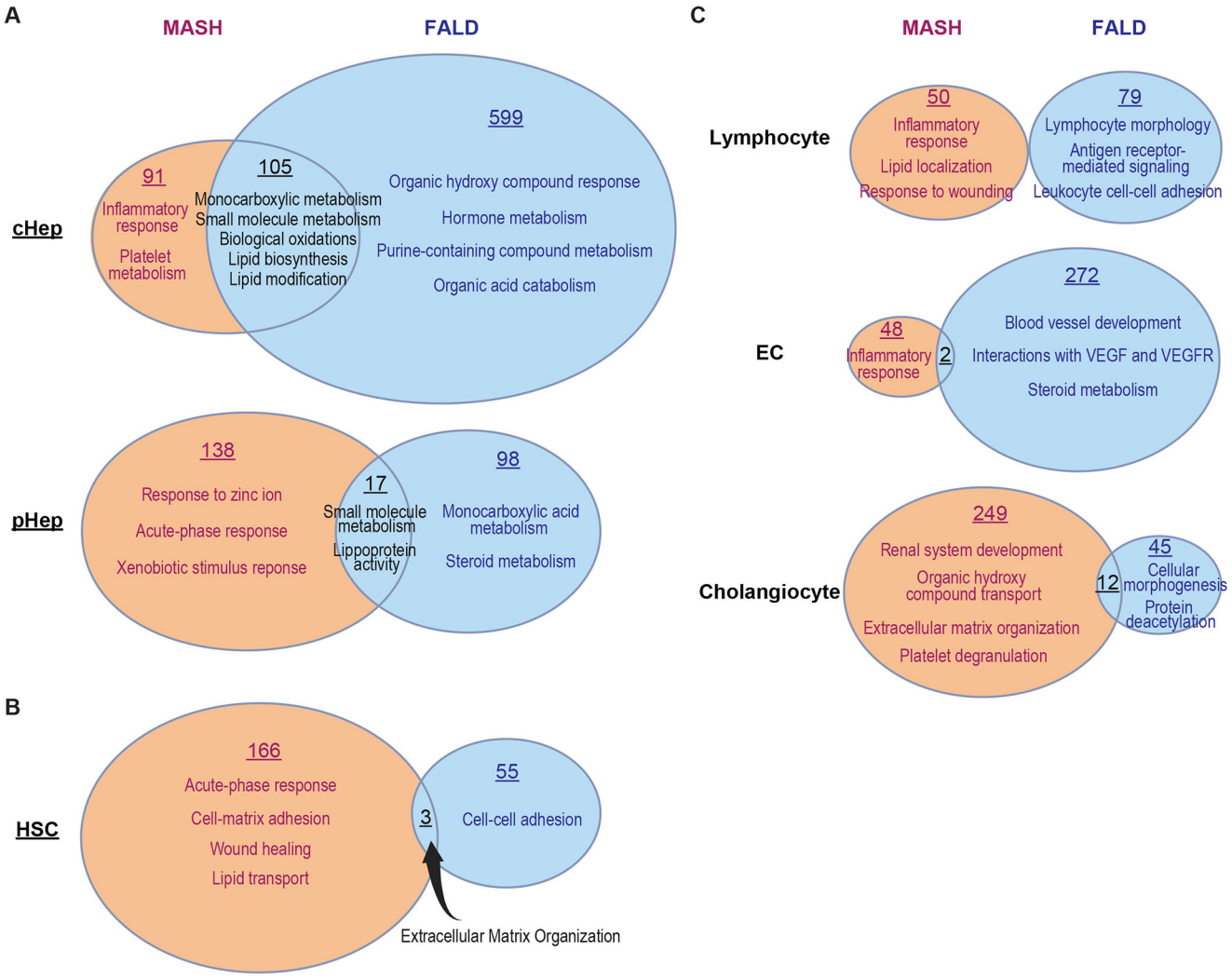

Fig. 6. Cell type-specific changes between FALD and MASH.

Venn diagrams showing unique and overlapping upregulated genes in MASH (n=9) (27) and FALD (n=4), in central hepatocytes (cHeps) and peripheral hepatocytes (pHeps) (**A**), HSCs (**B**), lymphocytes, ECs, and cholangiocytes (**C**). Number of genes are underlined. Enriched pathways ($P<1x10^{-5}$ and $\log_2$[fold change]>0.58) of unique and overlapping genes based on GO analysis are presented. EC and cholangiocyte overlapping genes showed no enriched pathways.